Caving 2026 – A van As, D Cumming-Potvin & J Wesseloo (eds)
© 2026 Australian Centre for Geomechanics, Perth, ISBN 978-1-7636842-3-2
doi:10.36487/ACG_repo/2645_47

The benefits of unconstrained, data-driven velocity models for seismic processing in caving operations

Imran Haque [a,*] , Wille Törnman [b,d], Jesper Martinsson [b], Catalina Vanegas-Palacio [a], Nico Viljoen [a], Avesiena Primadiansyah [c], Emil Svanberg [b]

[a] *Freeport-McMoRan, USA*

[b] *RockSigma, Sweden*

[c] *PT Freeport Indonesia, Indonesia*

[d] *Luleå University of Technology, Sweden*

Abstract

Microseismic monitoring is essential for panel caving operations, but a complex and changing environment makes it challenging to obtain accurate event location. This study evaluates an unconstrained, data-driven rock mass model (including velocity) for high-precision seismic processing at the Deep Mill Level Zone (DMLZ) panel cave in the Grasberg district. The approach uses the Bayesian estimation of mining-induced seismicity (BEMIS) framework, an automated, real-time system designed for the highly irregular and heterogeneous 'Swiss cheese' appearance of the underground rock mass. By combining Bayesian inference with adaptive calibration, event location accuracy and precision is improved, revealing clusters, structures and features that improve the understanding of cave propagation. The study also incorporates high-resolution P- and S-wave tomography by BEMIS, producing detailed velocity models with quantified uncertainties that enable data-quality filtering for reliable interpretation. The tomograms show low-velocity zones that closely match the evolving cave shape and high-velocity areas exhibiting stress accumulation, and highlight areas with poor ground conditions. In combination, the precise event locations and tomography provide new and valuable insights into cave evolution and extraction performance at the DMLZ. Overall, the study demonstrates that data-driven, Bayesian seismic processing offers a robust solution for precise velocity model estimation and cave monitoring in complex mining environments.

Keywords: *caving, seismic processing, data-driven velocity model, mining-induced seismicity, seismic tomography, event location accuracy*

1 Introduction

Microseismic monitoring is essential for safe and efficient operation of a cave, particularly in deep, high-stress environments. In caving operations, the rock mass is fractured, heterogeneous, and constantly changing as the cave grows. These conditions make achieving accurate seismic event location challenging. Yet, reliable locations are critical to understanding the cave propagation, assessing ground stability, managing geohazards and supporting production planning. A robust understanding of the evolving cave geometry is fundamental for mitigating major cave-related hazards such as rockbursts, airblasts, subsidence, and inrushes, all of which are strongly influenced by the extent of yielded and mobilised zones surrounding the cave.

Conventional seismic processing approaches often rely on fixed or constrained velocity models, which may not adequately represent the complex and time-dependent behaviour of the rock mass. Such constraints are commonly derived from assumed cave geometries and yielded zones, geological interpretations, or numerical modelling outputs. While this approach is generally more realistic than a non-informative homogeneous assumption, such constrained models can introduce biases, reduce the reliability of event

* Corresponding author. Email address: ihaque@fmi.com

locations and limit the ability to interpret evolving cave structures. Moreover, using seismicity data subsequently to update yielded zones or validate numerical models introduces a methodological risk, since the same models may already have been incorporated as prior assumptions.

To address these limitations, this study evaluates a fully data-driven approach that starts from an assumed homogeneous velocity model before inferring attenuation and wave velocities directly from the observed seismicity, as described in detail by Törnman & Martinsson (2020), Törnman et al. (2021), and Törnman (2021). The model updates continuously using passive data from thousands of events, blasts and mining noise triggers, and propagates uncertainties within a Bayesian framework into event locations and subsequent analyses (Martinsson 2013; Törnman et al. 2025). This results in a self-adapting representation of the evolving rock mass that is not dependent on imposed assumptions.

To demonstrate the self-calibrating approach, this study evaluates the accuracy and precision of blast-type event locations against known, mapped development blasts (described in Törnman et al. 2024). Establishing this reliability is a critical first step for interpreting seismicity. Building on these high-precision locations, the resulting seismic catalogue is used for passive 3D tomography (described in Törnman et al. 2025), producing detailed P-wave and S-wave velocity models together with associated quality metrics, such as ray density and velocity uncertainty. These models are generated at different timesteps to map evolving rock mass conditions and their relationship to features such as estimated cave geometry, uniaxial compressive strength (UCS) and rock quality designation (RQD).

The overall aim in this study is to evaluate whether time-lapse tomographic images with quality metrics, derived from reliable high-precision event locations, provide an additional, spatially continuous layer of information to support interpretation of cave geometry, stress redistribution and rock mass damage.

The work presented in this paper forms part of an ongoing effort to strengthen the technical basis for cave monitoring and geohazard management, rather than representing a finalised or fully implemented operational system.

2 Site overview: Deep Mill Level Zone panel cave

This section provides high-level context for the DMLZ panel cave, focusing on mining and cave setting, geotechnical environment and the seismic monitoring framework. Detail is intentionally limited to aspects most relevant for interpreting seismicity and rock mass behaviour.

The Grasberg mining complex, operated by PT Freeport Indonesia (PTFI), is located in the southern area of Jaya Wijaya Mountains, West Papua, Indonesia. Four mines are currently operating: 2 caving operations – the DMLZ and Grasberg block cave (GBC) mines, the Big Gossan stoping mine, and a third caving operation (Kucing Liar) is under development. Underground operations commenced in 1981 and the operation will extend to at least 2041. Figure 1 illustrates the general location of the different mines within the Grasberg mining complex.

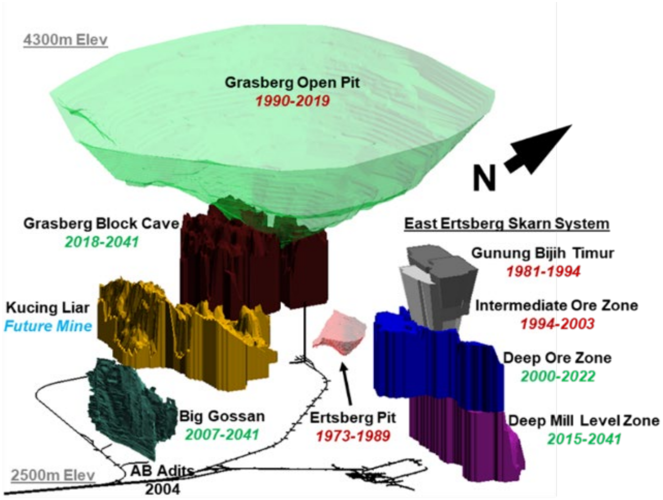

Figure 1 Overview of Grasberg mining district

2.1 Mining and cave setting

The DMLZ is the fourth cave mine within the East Ertsberg Skarn System (EESS). Each of the caves was developed as a new mining lift to extract increasingly deeper sections of the EESS. The DMLZ is located beneath the deep ore zone (DOZ) and approximately 1,500–1,800 m below surface, depending on steep topography. This places the DMLZ among the deepest operating block/panel caves globally (Simanjuntak et al. 2020).

2.1.1 Footprint and mining context

The DMLZ is a large-scale panel cave with an overall footprint approximately 1,500 m along strike and 700 m across strike. The planned footprint comprises approximately 2,300 drawpoints arranged in multiple production blocks. The mine was designed for peak production rates on the order of 80,000 tpd, with undercutting initiated in 2015 and a progressive ramp-up taking place through the late 2010s and early 2020s (Lolon et al. 2024).

Undercutting and caving have advanced progressively across multiple production blocks, including PB1, PB2, PB3 and PB4. PB4 is located at a higher elevation compared to the rest of the production block. Local adaptations to footprint geometry, undercut sequencing and pillar dimensions were made in response to observed ground behaviour and seismic response, see Figure 2.

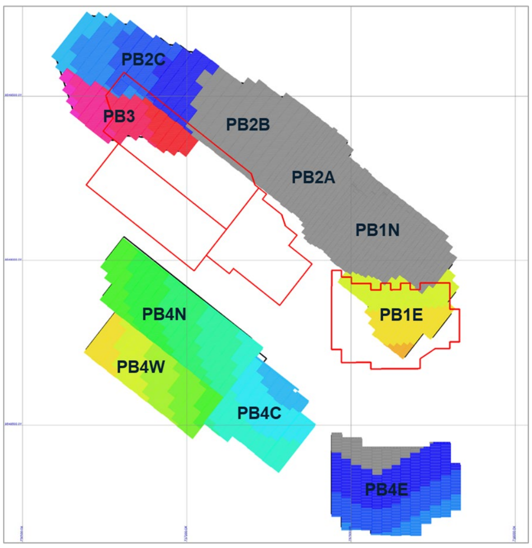

Figure 2 Future undercut sequence based on end 2025 10-K, where PB denotes production block

2.1.2 Cave interpretation

This section highlights the DMLZ cave interpretation workflow as it impacts the downstream analysis for cave management. As noted by Satriawan et al. (2025), PTFI has developed a level-of-confidence flow chart on building the cave shape. Visual inspections, undercut blasting and open hole data are higher confidence, while the spatial distribution is limited. Seismicity and tomography data are at a medium to low confidence rating. Therefore, defining tomographic data with regards to confidence is important in providing value for the interpretation for the cave shape.

The cave back definition with respect to seismic tomography can be referred to Duplancic & Brady (1999) in 3 zones: yielded, seismogenic and elastic zones. Seismicity or higher activity occurs in the seismogenic zone, whereas activity decreases further into the elastic zone. Comparing timelines of seismic activity may help determine the yielded zone, which ultimately aids in creating the cave shape due to cave propagation or movement.

2.1.3 Geological and geotechnical setting

The dominant lithologies at the DMLZ include Ertsberg diorite (Tertiary Ertsberg Intrusion), skarn, hornfels and local marble units. Diorite is the most extensive and mechanically competent unit, exhibiting high intact rock strength and low fracture frequency (UCS ~160 MPa and RQD >90), resulting in a strong, brittle rock mass. The skarn unit is generally weaker and more deformable, particularly near lithological contacts and faulted zones (see geology map in Figure 3). Across much of the footprint, the rock mass and especially the diorite is massive to sparsely jointed, such that stress-induced fracturing dominates over structurally controlled failure mechanisms.

At the depth of the DMLZ cave, in situ stresses are high, with a sub-horizontal major principal stress and magnitudes that increase approximately linearly with depth. These stresses are further perturbed by mining-induced stress redistribution associated with undercutting, cave growth and large-span development. In strong, brittle rock masses, this combination of high confinement and stress redistribution creates conditions conducive to strainbursting and dynamic failure when stress is not effectively managed.

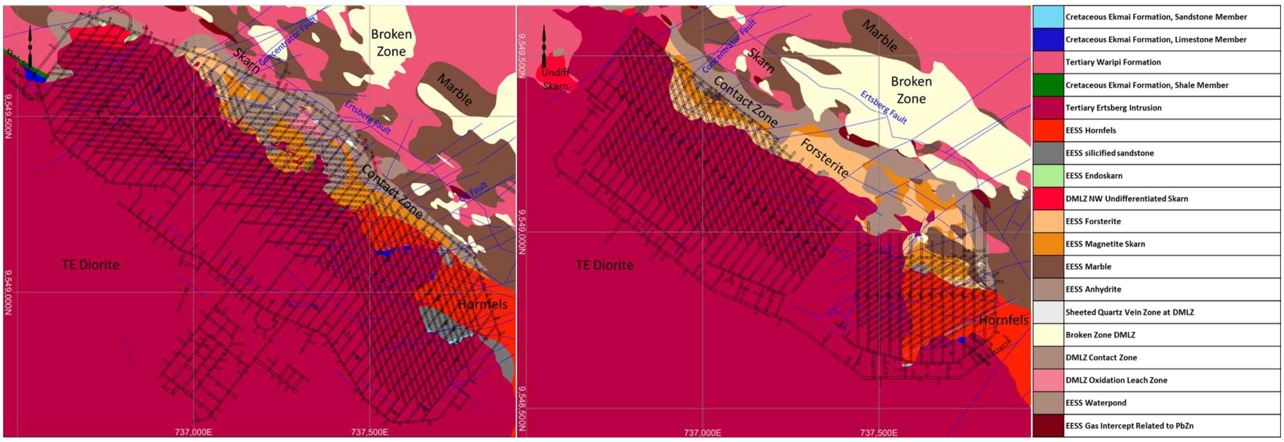

(a) (b)

Figure 3 (a) 2590 (PB1, PB2 and PB3) and (b) 2815 (PB4) extraction level geology

2.1.4 Seismic history and design response

A critical control on stress relief in caving operations is the timely and uniform propagation of the cave. At the DMLZ, early stages of undercutting and production ramp-up were characterised by delayed and locally inhibited cave propagation, particularly within the competent diorite units. Where cave growth stalled or progressed asymmetrically, stresses were not efficiently diverted around the caved rock mass but instead accumulated in abutment zones and pillars adjacent to the active footprint. This stress concentration reduced the expected stress-shadowing benefits of caving and increased the likelihood of brittle failure in development, undercut and extraction excavations.

These conditions motivated the implementation of advanced seismic monitoring at DMLZ, driven by the need to manage high in situ and mining-induced stresses, understand interactions between blasting and seismic response, control personnel exposure through exclusion and re-entry protocols, and track cave back position and propagation. Seismic data provide a critical proxy for cave growth and stall behaviour, directly informing cave management decisions and risk mitigation strategies.

The adverse stress conditions associated with delayed cave propagation manifested early in the mining sequence, particularly within PB1, where the initial DMLZ design was implemented. During early undercutting and ramp-up, several significant seismic events (Mw ≥2) occurred, resulting in damage to extraction level, undercut level, and associated infrastructure, periods of operational shutdown, and extensive rehabilitation requirements. These events highlighted the sensitivity of the strong diorite-dominated rock mass to stress accumulation in areas where cave propagation was delayed or incomplete (Lolon et al. 2024).

In response to this seismic behaviour, the original mine design and sequencing were progressively modified to better manage cave-induced stresses and promote more favourable cave growth conditions. Key changes included the transition from a narrow incline undercut layout to a W-undercut configuration, which was adopted to reduce stress concentrations in abutment zones and mitigate the damage and rockbursting observed in PB1 and portions of PB2 (Putra et al. 2024). This change was accompanied by a revised undercut sequence aimed at maintaining a rounded cave front, with the leading edge preferentially aligned along the diorite–skarn contact to improve caveability and reduce stress build-up along the cave margin.

Continuous monitoring of cave growth and cave shape became a central element of seismic risk management. Interpreted cave geometry was used to assess stress redistribution around the undercut and extraction levels and to inform adjustments to development sequencing and focus production where cave propagation lagged. These adjustments were implemented alongside enhanced ground support systems, updated maintenance and rehabilitation strategies, and the use of hydraulic fracturing to promote cave growth and improve stress redistribution ahead of the cave front.

While these design and sequencing changes did not eliminate seismicity, they significantly improved the mine's ability to manage seismic risk, reduce the frequency and severity of damaging events, and maintain operational continuity under high-stress conditions.

2.1.5 Seismic monitoring system and data application

A permanent underground microseismic monitoring system is used to continuously record the rock mass response to mining-induced stress changes. The system consists of a distributed network of underground sensors arranged to provide three-dimensional coverage of the active mining areas and evolving cave volumes (see Figure 4). The network layout is limited by accessibility but designed to detect, locate and characterise seismic events associated with stress redistribution, rock mass damage and cave propagation.

The seismic network employs underground sensors capable of detecting microseismic to larger-magnitude events. Data is continuously transmitted and processed in near real-time by commercial seismic processing platforms, generating large volumes of data that require automated detection, location and quality control workflows. Operational constraints include sensor survivability in high-stress environments, access limitations for installation and maintenance, and interference from mining-related noise.

3 Methodology

The approach applied at the DMLZ panel cave is implemented using BEMIS, a fully automatic, near real-time, self-learning platform for induced seismicity (Törnman & Martinsson 2020). BEMIS applies Bayesian statistics and Markov chain Monte Carlo (MCMC) methods rather than deterministic models (Martinsson 2013), representing all parameters as probability distributions to provide realistic uncertainty estimates throughout the workflow. The self-learning component automatically adjusts for biases in attenuation, spectral properties and P- and S-wave velocities (Törnman & Martinsson 2020; Törnman et al. 2021; Törnman 2021).

The resulting seismic catalogue, including uncertainties, provides confidence-filtered data for sequential analyses such as passive tomography (Törnman et al. 2025). These data are used to produce 3D models of Vp and Vs, with associated uncertainty estimates and ray-box intersections per grid cell on a monthly basis. These models are designed to support geotechnical interpretation, including the assessment of stress concentrations, remnant pillars and stalled caving (Törnman et al. 2025).

4 Results and discussions

This section presents results of the BEMIS seismic catalogue, demonstrating improvements in seismic event location and velocity tomography, and their application to cave monitoring. Enhanced location precision and clustering reveal previously unresolved seismic features to improve tracking of cave geometry and propagation. These results are followed by tomographic images that illustrate the spatial and temporal evolution of rock mass damage and stress redistribution.

4.1 Improvements in event location

To quantify the effects of self-calibration, events classified as blast within a selected area slightly larger than the boundaries shown in Figure 5 were analysed, constrained to the vertical interval between 2,700 m and 2,900 m depth. Given that this area is far away from the cave, and the geophone coverage is good, the rock mass is expected to be relatively homogeneous, and the impact of self-calibration should be limited and can therefore be seen as a least influential case. These blast events (i.e. 1,583 blast events) were processed using both a homogeneous velocity model (Vp = 5,300 m/s, Vs = 3,100 m/s), and the self-calibrated velocity model.

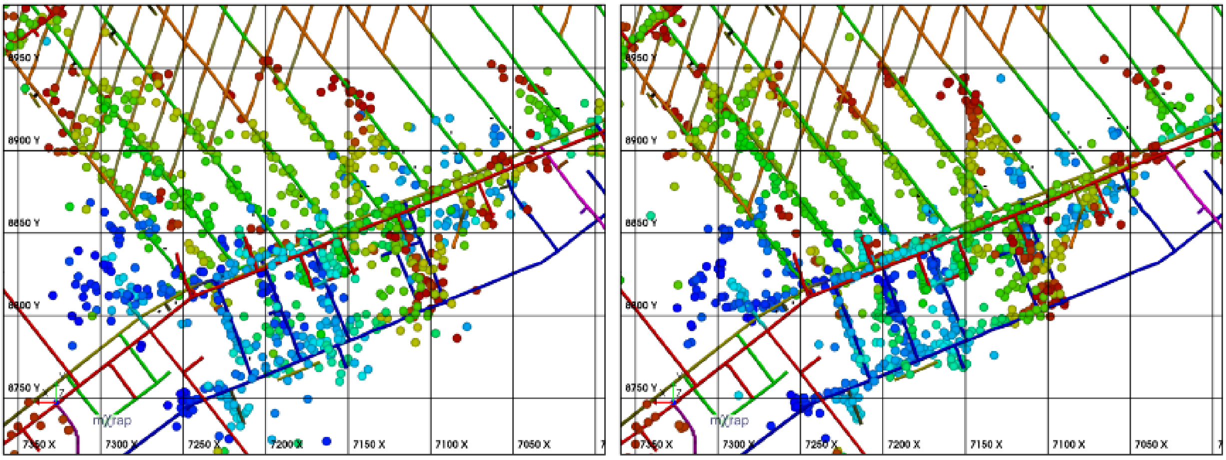

(a) (b)

Figure 4 Hypocentre locations of events classified as blast coloured by date, recorded between 1 January 2025 (blue) and 1 December 2025 (red). (a) Located events using homogenous velocity model; (b) Location using BEMIS self-calibrated velocity

The self-calibrated model detected approximately 17% more blast events. Additionally, the median location error relative to the mapped development blasts decreased from 11.6 m to 6.4 m. The median is preferred to reduce the influence of outliers, as the match between an event and the corresponding blast is uncertain due to inexact blast time knowledge, which can differ by almost 1 hour from set actual blast time. Since BEMIS segments individual seismograms from a single development blast sequence, multiple event locations can be generated from that one sequence and mapped to the same blast coordinate (Törnman et al. 2024). This provides valuable information daily about the precision and accuracy of the system without requiring a dedicated validation blast. This improvement is clearly visible in the hypocentre clustering shown in Figure 4, where the self-calibrated model (Figure 4a) is less scattered with respect to the drifts, compared to the homogeneous model (Figure 4b). Improved seismic event location accuracy supports the cave shape interpretation and overall seismic risk management as outlined in the relevant trigger action response plans (TARPs).

Accurate and precise event locations are essential for reliably describing the cave geometry. To highlight this, an interpreted cave shape, preceding the timeframe of the BEMIS-located events, is shown in Figure 5. The events are coloured by date, and distinct spatiotemporal clusters are clearly visible. The more recent events tend to occur farther away from the interpreted cave (see the horizontal XY view, Figure 5a) which indicates the progressive cave growth over time. Having precise seismic event locations is important in tracking cave propagation.

Another notable observation from the vertical XZ section is the close similarity in shape between the distribution of the oldest events (blue dots) and the cave model. The events are offset from the cave model. Some offset is expected as the seismogenic zone is typically located some distance away from the yielded (caved) zone (Duplancic & Brady 1999).

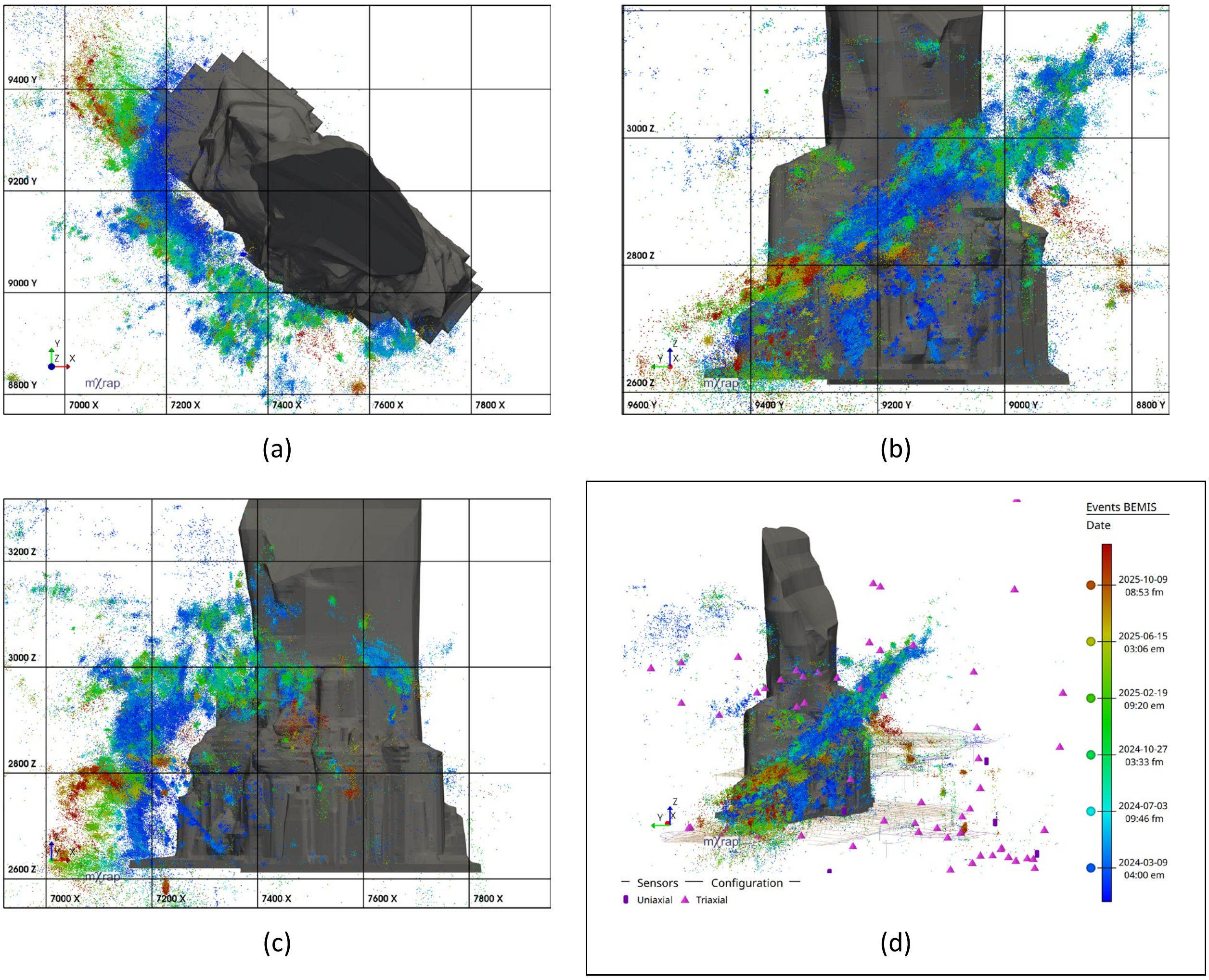

Figure 5 **Hypocentre locations of accepted BEMIS events recorded between 1 January 2024 and 1 January 2026, filtered to include events with a location uncertainty ≤13.3 m and coloured by date. The figure also shows the cave geometry at January 2024**

4.2 Velocity tomography results

This section presents the velocity tomography results for key areas of the cave over time. Figure 6 shows a horizontal section at the 2,700 m elevation, 100 m above the PB1-PB2 undercut level. For each section, P-wave and S-wave velocity models are compared with geological and geotechnical features, including lithological contacts, the DMLZ broken zone, EESS marble, diorite and mapped faults, together with available UCS and RQD block models. Mining-related features such as cave geometry, development progress and undercut advance are also included to provide operational context. The section is presented as annual snapshots from 2024 to 2026, allowing assessment of the spatial and temporal evolution of velocity structure in relation to geology and mining progression.

The tomograms in Figure 6 are presented without quality filtering. Consequently, areas not intersected by rays in current or historical time-slices retain the initial velocity assumptions (i.e. P-wave velocity of 5,297 m/s and S-wave velocity of 3,061 m/s, shown as green areas), which are estimated as the mean ray velocities (Törnman et al. 2025). Instead, quality plots are shown in Figure 7 to show where the data are consistent and have sufficient ray coverage, respectively.

Figure 6 shows a horizontal slice at depths of 2,700 m (100 m above the PB1-PB2 undercut level), providing a plan view perspective of cave-related damage and stress redistribution. In 2024, the low-velocity zone extends slightly beyond the northwestern end of the interpreted cave footprint, suggesting damage or yielding propagating ahead of the modelled cave front in this direction. In contrast, elevated velocities persist within the estimated cave toward the southeastern end, indicating areas that had not yet fully mobilised at that stage. By January 2025, and more clearly in January 2026, the distribution of low-velocity anomalies aligns more closely with the modelled cave geometry. Higher velocities remain concentrated in the surrounding abutments, particularly within the diorite, consistent with stress concentration and confinement adjacent to the cave margins.

Since the cave model later expanded to include the low-velocity areas, it is possible that the 2024 cave interpretation underestimated the cave's actual extent. Additional support comes in Figures 5a and 5c which shows the seismogenic zone in 2024 represented by blue hypocentres. These clusters extend beyond the modelled cave (grey), and the gap between the modelled cave and the seismogenic zone could suggest a larger yielded zone than initially inferred. Overall, these observations indicate that combining precise event locations with tomographic data can provide valuable insight into the evolving cave geometry and may help identify areas where direct measurements, such as drillhole camera inspections, could be beneficial.

In January 2024, the number of seismic rays was more than 6 times greater than in January 2026, and fat rays were used in the inversion to provide a smooth and stable starting model for the monthly tomographic images. Sequential months then used thin rays to reduce processing time. The reduced ray density in 2026 increases 'salt-and-pepper' artefacts in the tomograms, particularly visible in the footwall (Figure 6, where the 2024 January model appears smooth, while the 2026 January model shows closely spaced low-velocity and high-velocity anomalies). Lower ray coverage reduces spatial stability and increases sensitivity to local variations in the inversion. This effect could be reduced by increasing ray coverage, for example by using longer time periods, including more uncertain events, or applying fat rays.

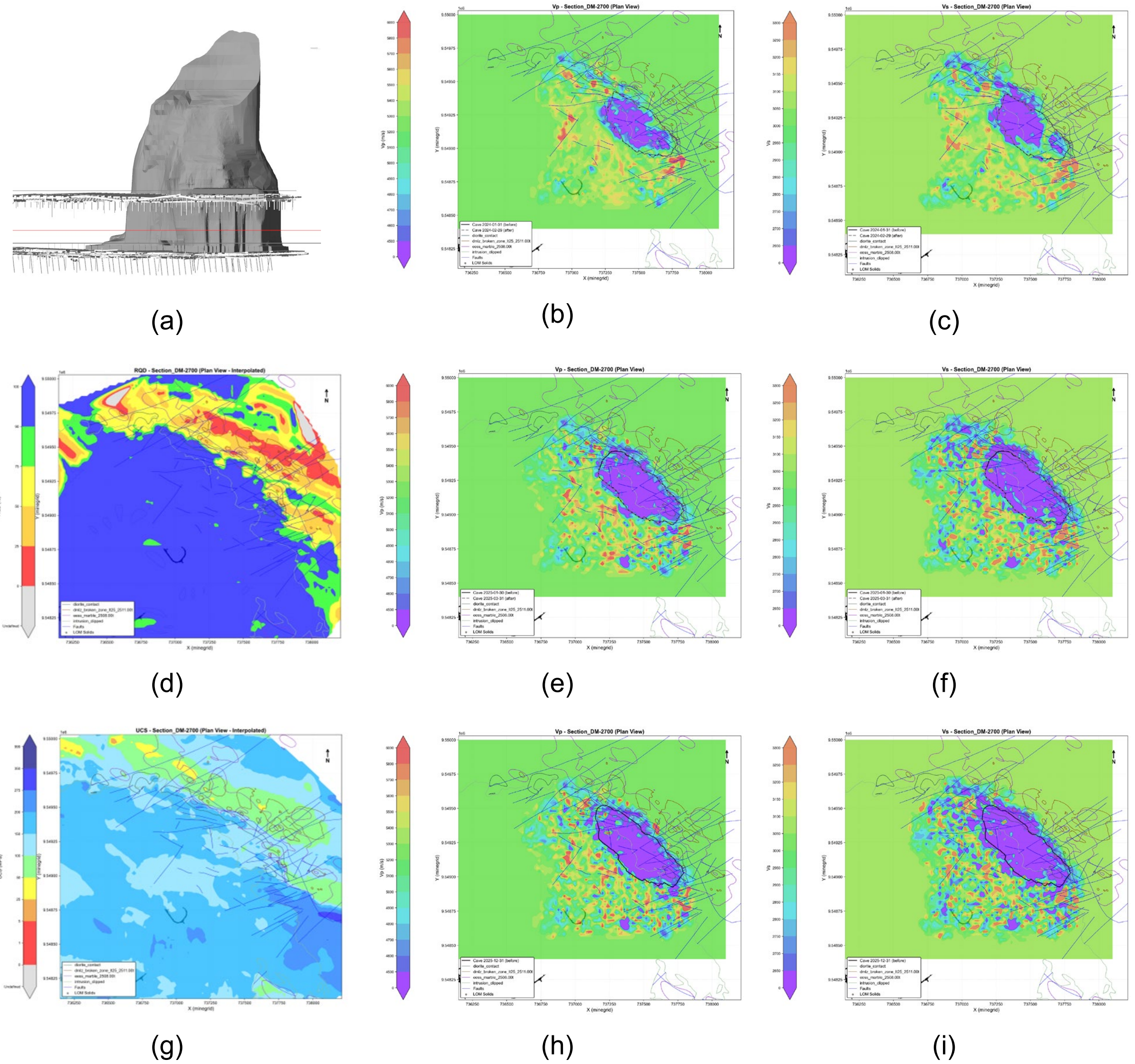

Figure 6 Velocity tomography results along the 2700 level, 100 m above the PB1-PB2 undercut over time. (a) Section location; (b) and (c) P-wave velocity (Vp) and S-wave velocity (Vs) in January 2024; (d) Rock quality designation along the section; (e) and (f) Vp and Vs in January 2025; (g) Uniaxial compressive strength along the section; (h) and (i) Vp and Vs in January 2026

4.3 Velocity estimation and confidence metrics

The interpretation of tomography results is typically focused on the wave velocity while the complete dataset includes a wider range or parameters. For each grid cell, the following parameters are provided:

- Vp, Vs: P-wave and S-wave velocities
- σVp, σVs: standard deviations of the inverted velocities
- Np, Ns: number of intersecting P- and S-wave rays.

The Vp and Vs are presented as absolute values with no reference to the information supporting each of the interpretation.

Confidence in the inverted velocities should be based on the underlaying data and can be broadly interpreted as:

- High N, low σV: many rays with high agreement -> high confidence.
- High N, high σV: many rays with low agreement -> high variability.
- Low N, low σV: few rays with high agreement -> low confidence.
- Low N, high σV: few rays with low agreement -> very low confidence.

As mentioned in earlier sections, creating the DMLZ cave shape is dependent on the monitoring tools and their confidence levels. The tomographic imaging of seismic wave velocities requires additional investigation on confidence ratings.

A proposed confidence methodology that is applied has 2 variables: number of rays (Np) and variability (σ). As shown in Figure 7, both variables are evaluated to determine the confidence of the Vp and whether it is suitable for cave shape interpretation.

A confidence range was established based on a statistical analysis of monthly data to capture expected variations in cave behaviour. Outliers and pre-defined caving or yielding velocity thresholds were applied to ensure the range reflects physically meaningful conditions. This confidence range is used solely for interpretation confidence and is independent of seismic velocity dispersion metrics.

A few important points to note:

- Long rays distribute information over larger regions, reducing local spatial confidence (despite high N and low σV).
- Many rays from a single source or to a single sensor may provide many intersections but limited directional coverage reduces the ability to resolve unique velocities along that path (despite high N and low σV).
- Zones without ray intersections (N = 0) may indicate highly damaged or yielded rock, as seismic rays bend around these low-velocity areas; high-variability zones are naturally occurring at cave boundaries.

To address these limitations, additional metrics are currently under evaluation. These include statistical measures such as the Cramér–Rao lower bound, quantification of directional diversity, and comparisons between observed ray density and a theoretical homogeneous distribution to identify ‘ray avoidance’. Integrating these metrics into a single unified measure would be a valuable objective for simplifying interpretation for general users; however, these individual measures may also provide useful information that can help strengthen conclusions for expert users. Ray coverage also limits temporal resolution. Averaging over multiple months can stabilise tomograms in poorly covered areas but smooths temporal changes. Increasing rays by lowering event quality thresholds risks introducing outliers. Another solution is to use fat ray tomography which provides more coverage at the cost of spatial smoothing and increased computational load. Another more effective strategy is to employ active sources, such as mobile scaling machines, which can be strategically deployed to illuminate important areas lacking ray coverage or directional diversity (Törnman et al. 2025).

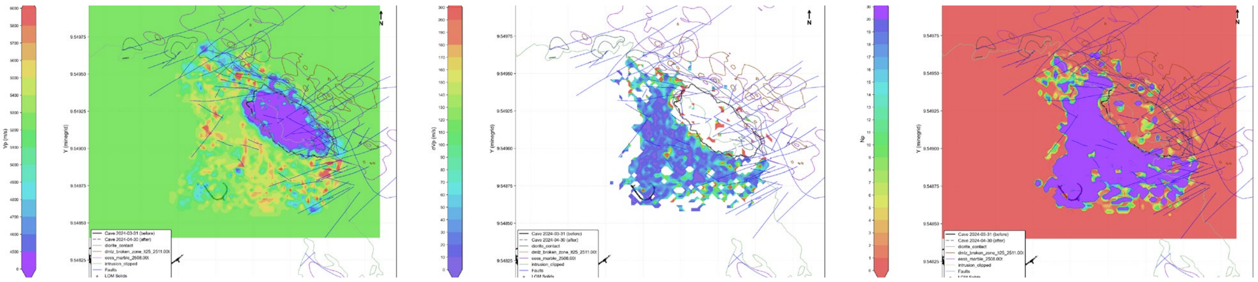

(a) (b) (c)

Figure 7 Velocity tomography results along the 2700 level, 100 m above the PB1-PB2 undercut in March 2024. (a) P-wave velocity (Vp); (b) P-wave velocity variability (σVp); (c) Number of rays (Np)

5 Conclusion

This study evaluated a fully data-driven, unconstrained approach to seismic processing at the DMLZ panel cave using the BEMIS framework. The velocity model is inferred directly from observed seismicity without imposed assumptions on cave geometry or rock mass properties.

Compared to a homogeneous velocity model, the self-calibrated model reduced the median blast location error from 11.6 m to 6.4 m and detected approximately 17% more blast events at the quality threshold. The improved locations result in tighter hypocentre clustering of the blast events and seismic event locations. This feature is important for the understanding of cave propagation and overall seismic risk management.

The high-precision locations were used as input for passive 3D tomography. The resulting Vp and Vs models show reasonable spatial correlation with low-velocity zones and the cave boundary, while higher velocities are observed in abutment zones where stress concentration would be expected. Time-lapse tomograms from 2024 to 2026 indicate a progressive expansion of low-velocity anomalies that seems consistent with cave propagation and rock mass damage.

Preliminary back-analysis of the tomography data highlighted low-velocity zones that extended beyond the boundaries of cave as previously interpreted from traditional monitoring systems. Subsequent cave shape interpretations expanded into these areas, suggesting that the tomography captured cave growth earlier than the conventional interpretation. This suggests that tomographic imaging could be a useful tool to supplement other monitoring tools for cave shape estimation, though further validation is needed.

The reliability of the tomograms depends on ray coverage. Where coverage is good, the images appear stable and consistent, with promising correlation to the interpreted cave shapes. In areas with fewer rays, particularly in the 2026 models, spatial artefacts become more apparent. Ongoing work is focused on using the available parameters to define the data confidence and avoid misinterpretation in low-confidence areas.

Overall, this data-driven Bayesian approach has strong potential for broader application in cave monitoring, as it is fully automatic and does not require calibration blasts or predefined cave models, thereby avoiding circularity when the results are used to interpret cave geometry. The results align with the cave shape model constructed using additional, independent metrics (e.g. visual inspections, open hole data, Elexon data and other geotechnical indicators) and could support cave shaping and its downstream analyses.

Acknowledgement

The authors would like to acknowledge the assistance of the PTFI and strategic planning teams for their support in preparing this paper and to the larger PTFI organisation for permission to publish this paper. The authors would also like to acknowledge the data provided and access by the seismic data provider.

References

Duplancic, P & Brady, BH 1999, 'Characterisation of caving mechanisms by analysis of seismicity and rock stress', *Proceedings of the 9th Congress of the International Society for Rock Mechanics*, CRC Press/Balkema, Paris, pp. 1049–1053.

Lolon, S, Campbell, R, Edgar, I, Priatna, A & Haque, I 2024, 'Implementation of major mining strategy changes at the Deep Mill Level Zone (DMLZ) mine, PT Freeport Indonesia', in D Johansson & H Schunnesson (eds), *MassMin 2024: Proceedings of the International Conference & Exhibition on Mass Mining*, Luleå University of Technology, Luleå, pp. 73–85, https://doi.org/10.36487/ACG_repo/2435_A-07

Martinsson, J 2013, 'Robust Bayesian hypocentre and uncertainty region estimation: the effect of heavy-tailed distributions and prior information in cases with poor, inconsistent and insufficient arrival times', *Geophysical Journal International*, vol. 192, no. 1, pp. 1156–1178.

Putra, F, Perdana, A, Hamman, J & Campbell, R 2024, 'A geotechnical review of the transition from narrow incline undercut to w-undercut design at the Deep Mill Level Zone mine, PT Freeport Indonesia', in P Andrieux & D Cumming-Potvin (eds), *Deep Mining 2024: Proceedings of the 10th International Conference on Deep and High Stress Mining*, Australian Centre for Geomechanics, Perth, pp. 1319–1334, https://doi.org/10.36487/ACG_repo/2465_87

Satriawan, E, Munandar, A, Immanuela, R, Primadiansyah, A, Soumilena, A & Meiharriko N 2025, 'Potential cave shape interpretation through a comprehensive monitoring system at the Deep Mill Level Zone Mine, Indonesia', *Proceedings of the ARMA Symposium*, American Rock Mechanics Association, Alexandria.

Simanjuntak, K, Primadiansyah, A, Soumilena, N & Teweng, W 2020, 'Driving and managing stress in the Deep Mill Level Zone caving mine', in R Castro, F Báez & K Suzuki (eds), *MassMin 2020: Proceedings of the Eighth International Conference & Exhibition on Mass Mining*, University of Chile, Santiago, pp. 394–405, https://doi.org/10.36487/ACG_repo/2063_25

Törnman, W 2021, *Towards Reliable Seismic Hazard Assessment in Underground Mines,* PhD thesis, Luleå University of Technology, Luleå.

Törnman, W & Martinsson, J 2020, 'Reliable automatic processing of seismic events: solving the Swiss cheese problem', in J Wesseloo (ed.), *UMT 2020: Proceedings of the Second International Conference on Underground Mining Technology*, Australian Centre for Geomechanics, Perth, pp. 155–172, https://doi.org/10.36487/ACG_repo/2035_04

Törnman, W, Martinsson, J & Dineva, S 2021, 'Robust Bayesian estimator for S-wave spectra using a combined empirical Green's function', *Geophysical Journal International*, vol. 227, no. 1, pp. 403–438.

Törnman, W, Martinsson, J & Svanberg, E 2024, 'Enriching seismic data with noise and blasts and the importance of credibility', in P Andrieux & D Cumming-Potvin (eds), *Deep Mining 2024: Proceedings of the 10th International Conference on Deep and High Stress Mining*, Australian Centre for Geomechanics, Perth, pp. 207–216, https://doi.org/10.36487/ACG_repo/2465_08

Törnman, W, Martinsson, J & Svanberg, E 2025, 'High-resolution tomographic investigation at the Kiruna Mine prior to a major seismic event', *Proceedings of the 11th International Symposium on Rockbursts and Seismicity in Mines*, Luleå University of Technology, Luleå, pp. 558–578.